MOLECULAR IMAGING AND BIOLOGY

Mol Imaging Biol (2013) 16:311–316
DOI: 10.1007/s11307-013-0702-3

Published Online: 9 November 2013

World Molecular Imaging Society

BRIEF ARTICLE

Performance Evaluation of Stationary and Semi-Stationary Acquisition with a Non-Stationary Small Animal Multi-Pinhole SPECT System

Catharina Lange,[1] Ivayla Apostolova,[1,2] Mathias Lukas,[1,3] Kai P. Huang,[1] Frank Hofheinz,[4] Betina Gregor-Mamoudou,[1] Winfried Brenner,[1] Ralph Buchert[1]

[1]*Department of Nuclear Medicine, Charité - Universitätsmedizin Berlin, Charitéplatz 1, 10117 Berlin, Germany*
[2]*Present Address: Department of Radiology and Nuclear Medicine, Otto-von-Guericke University, Leipziger Str. 44, 39120 Magdeburg, Germany*
[3]*Present Address: Department of Nuclear Medicine, Technical University Munich, Klinikum rechts der Isar, Ismaninger Straße 22, 81675 Munich, Germany*
[4]*Institute of Radiopharmaceutical Cancer Research, PET Centre, Helmholtz-Zentrum Dresden-Rossendorf, Bautzner Landstraße 400, 01328 Dresden, Germany*

Abstract

Purpose: Step-and-shoot mode with many angular steps results in long frame duration limiting the capability of single-photon emission computed tomography (SPECT) for fast dynamic scans. The present study evaluates acquisition with reduced angular sampling for fast imaging in preclinical research with the nanoSPECT/CTplus four-head multi-pinhole system.

Procedures: Measurements with line sources, homogeneity phantoms and a Jaszczak phantom filled with ^{99m}Tc or ^{123}I were performed to evaluate the 'stationary' and 'semi-stationary' acquisition mode (one or two detector positions, respectively) with respect to spatial resolution, quantification, noise properties and image artefacts. An *in vivo* mouse study was performed with ^{99m}Tc-MAG3.

Results: The fast acquisition modes resulted in only minor degradation of spatial resolution and quantification accuracy. Statistical noise in reconstructed images was significantly reduced compared to conventional SPECT, particularly at low count statistics. Stationary acquisition resulted in streak artefacts and spatial distortion.

Conclusions: The semi-stationary acquisition mode of the nanoSPECT/CTplus allows fast dynamic SPECT with tolerable loss of image quality.

Key words: SPECT, Dynamic imaging, Stationary, Performance evaluation

Introduction

Characterization of the pharmacokinetics of new tracers as a part of their preclinical evaluation is an important application of small animal positron emission tomography (PET) and single-photon emission computed tomography (SPECT) [1, 2]. The time course of the concentration of a radiotracer in the organs of interest is tracked by dynamic imaging, i.e., acquisition of a sequence of images (frames) starting with the injection of the tracer. Short frames are required to provide adequate temporal sampling, particularly after injection when the initial tissue distribution occurs. In case of small animal SPECT, the capability for short frames is limited by photon counting sensitivity, despite the use of multiple heads and multi-pinhole apertures [3, 4]. Sensitivity

Electronic supplementary material The online version of this article (doi:10.1007/s11307-013-0702-3) contains supplementary material, which is available to authorized users.

Correspondence to: Ralph Buchert; *e-mail:* ralph.buchert@charite.de

for high-resolution SPECT in the mouse is approximately 1 per mille (1 cps/kBq), i.e., about 2 orders of magnitude smaller than in small animal PET [5].

Small animal pinhole SPECT systems based on a small number of large, conventional scintillation detectors (intrinsic resolution ≥2 mm) allow high magnification of the projection image in order to achieve high spatial resolution. A disadvantage of this design is that the gantry has to be rotated during the SPECT acquisition in order to obtain sufficient angular sampling. This further reduces the effective counting sensitivity by the 'dead time' during detector motion, which is considerable in conventional step-and-shoot mode with many angular steps.

Dead time due to detector motion can be avoided by using a large number of small detectors arranged around the animal for simultaneous acquisition of all projections. This has been realized in stationary SPECT systems which do not require detector motion [6–9].

In conventional, i.e., non-stationary small animal SPECT systems, dead time due to detector motion might be reduced by decreasing the number of detector positions. The resulting angular undersampling can be minimized by the use of multi-pinhole apertures: the holes are drilled in different directions so that each hole defines a different projection angle. The reduction of the number of detector positions has a second effect with the potential to improve the capability for fast dynamic imaging: the total number of counts detected during a short time interval is allocated to a smaller number of projections. Each of this small number of projections has better statistical quality than each of a larger number of projections acquired in the same time interval. This reduces statistical noise in the reconstructed images which in turn allows reduction of the net frame duration (A small number of good quality projections provides more information than a large number of projections which contain mainly noise.).

However, reduced angular sampling causes degradation of image quality and occurrence of specific artefacts in the reconstructed images, the severity of both these phenomena depending on the extent of the undersampling. It is to be expected that there is a well-defined minimum number of detector positions required to keep image degradation tolerable. Image degradation becomes significant only when the number of detector positions is reduced below this threshold, which should depend on the SPECT system and the collimators used.

The aim of the present study was to evaluate the effect of angular sampling for the (non-stationary) nanoSPECT/CTplus small animal system (*Bioscan*, *Washington*, *DC*, *USA*) [10–12]. The SPECT component is based on a four-head SPECT camera for brain imaging in humans. Each of the four large NaI(Tl) scintillation detectors can be equipped with a multi-pinhole aperture. The nanoSPECT/CTplus provides a 'stationary' acquisition mode without detector motion and a 'semi-stationary' mode with two detector positions displaced by 45 °. Phantom measurements were performed to evaluate these acquisition modes with respect to spatial resolution, quantification, noise properties and image quality as assessed by visual inspection. A dynamic SPECT scan with initially 20 s frames after intravenous (i.v.) injection of ^{99m}Tc-MAG3 (^{99m}Tc-mercaptoacetyltriglycine) in the mouse was performed to demonstrate the potential for fast dynamic SPECT with good image quality. ^{99m}Tc-MAG3 is the standard radiopharmaceutical for qualitative and quantitative estimation of renal clearance and kidney excretion, and is often used for the diagnosis of obstructive uropathies in children and monitoring of their treatment (13). ^{99m}Tc-MAG3 shows very fast pharmacokinetics which makes it a particularly challenging tracer for dynamic SPECT.

Materials and Methods

Measurements were performed with the isotopes ^{99m}Tc and ^{123}I and four sets of nine-pinhole apertures: rat high resolution (RH), pinhole diameter d=1.5 mm; rat ultra-high resolution (RU), d=0.8 mm; mouse high resolution (MH), d=1.0 mm; and mouse ultra-high resolution (MU), d=0.5 mm. Images were reconstructed with the ordered subsets-expectation maximization algorithm of the system software HiSPECT (*Bioscan*, *Washington*, *DC*, *USA*). Standard parameter settings (three subsets; three iterations; smoothing, 35 %) were used in all cases except for the Jaszczak phantom (eight subsets; three iterations; smoothing, 25 %).

Spatial Resolution

A glass capillary tube with inner diameter of 1.0 mm was filled with ~50 MBq/ml of ^{99m}Tc or ^{123}I. The capillary was aligned in

Table 1. Spatial resolution: mean±standard deviation of FWHM [in millimetre]

Isotope	Scan mode	Aperture			
		RH	RU	MH	MU
^{99m}Tc	Conventional	1.16±0.01	0.82±0.02	0.69±0.01	0.62±0.01
	Semi-stationary	1.24±0.05	0.86±0.02	0.71±0.02	0.62±0.01
	Stationary	1.24±0.06	0.92±0.02	0.76±0.02	0.65±0.04
^{123}I	Conventional	1.17±0.02	0.86±0.01	0.73±0.02	0.66±0.03
	Semi-stationary	1.26±0.03	0.84±0.03	0.71±0.02	0.64±0.01
	Stationary	1.30±0.06	0.98±0.05	0.82±0.04	0.70±0.02

FWHM full-width-at-half-maximum, *RH/RU* rat high/ultra-high resolution, *MH/MU* mouse high/utra-high resolution

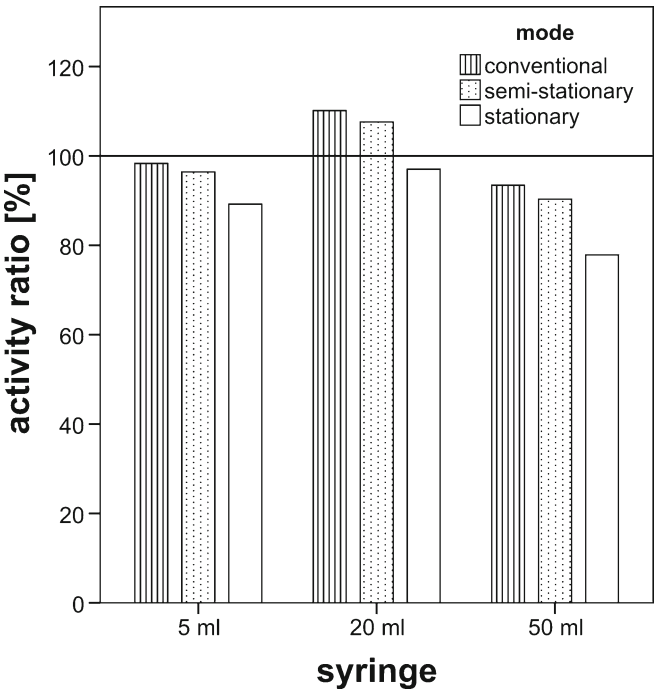

Fig. 1. Quantification performance of semi-stationary and stationary acquisition mode compared to conventional mode for homogeneity phantoms (syringes) of different size filled with ^{99m}Tc. The total activity in the SPECT image is given relative to the true total activity in the syringe (activimeter measurement) in percent. The 5-ml syringe was scanned with aperture MH, the 20 and 50 ml ones with aperture RH.

axial direction at the centre of the transaxial field of view (FOV). The axial FOV was set to the maximum axial FOV of the stationary mode in all cases (22 mm for rat, 14 mm for mouse apertures).

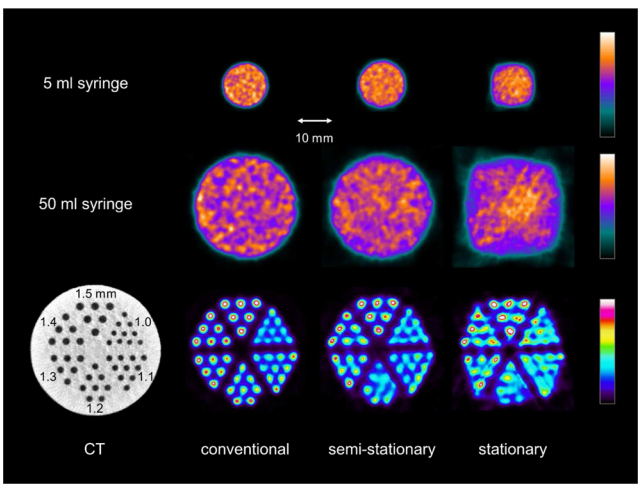

Fig. 2. Representative transaxial slice through the SPECT of syringes (*upper row*, 5 ml syringe with aperture MH; *middle row*, 50 ml syringe with aperture RH) and a 1.0–1.5-mm internal diameter Jaszczak phantom (*lower row*, aperture RH) acquired in conventional, semi-stationary and stationary mode. Spatial distortions and streak artefacts are prominent in the strictly stationary mode, more pronounced in the 50 ml than in the 5 ml syringe.

SPECT was performed in each mode (conventional with 10 angular positions, semi-stationary and stationary) with every aperture–isotope combination. Each scan was repeated two times resulting in three scans in order to improve statistical reliability of the results. The spatial resolution was determined from the transaxial intensity profile through the line source separately for vertical and horizontal direction [14]. After correcting the profile for the source dimension via deconvolution with a rectangular window of 1.0 mm width, a Gaussian fit was performed to obtain the full-width-at-half-maximum (FWHM). Vertical and horizontal FWHM were averaged, as there was no relevant difference. The resulting FWHM was averaged over 40 consecutive transaxial slices, as there was no relevant variation over the covered interval in axial direction.

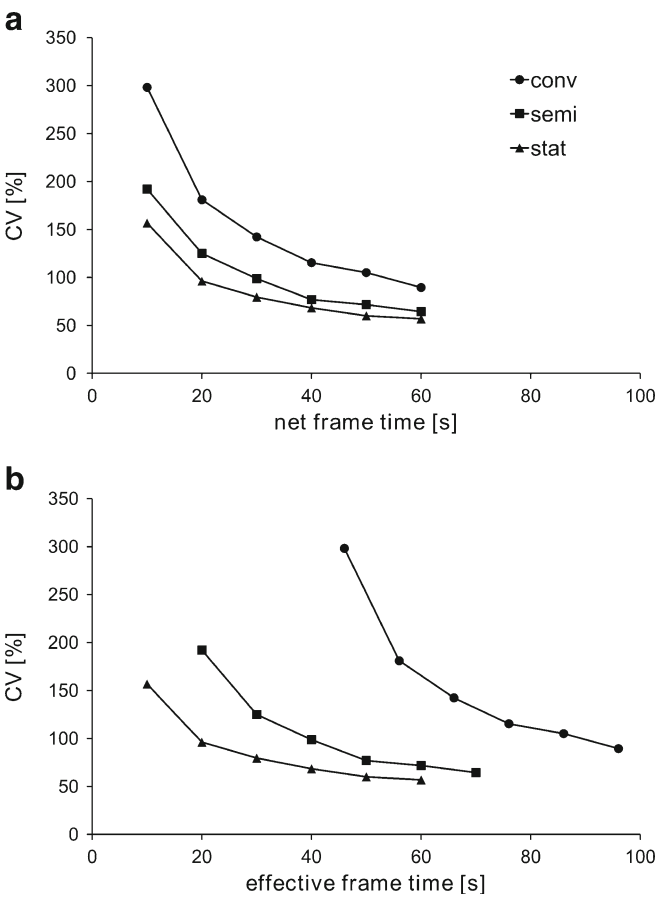

Fig. 3. Impact of the acquisition mode on noise propagation. The coefficient of variance (*CV*) of the voxel intensities within a homogeneity phantom (5 ml syringe) was used to characterize the level of noise in the reconstructed image. The CV is plotted as function of the frame time, either the net frame time (**a**), which is the actual duration of the data collection without dead time during detector motion, or as function of the effective frame time (**b**), which is the total duration of the frame including the dead time during detector motion (effective time=net time+dead time). In the conventional acquisition mode with 10 angular positions, the effective frame time is 36 s longer than the net frame time (about 4 s for each rotation of 18°). In semi-stationary mode, the difference is about 10 s (for one rotation of 45°). (conv/semi/ stat=conventional/semi-stationary/stationary acquisition mode).

Calculations were performed with MATLAB (*The Mathworks*, *Inc*., *Nattick*, *MA*, *USA*).

Quantification

The SPECT system was calibrated prior to the experiment for ^{99m}Tc and all apertures according to the manufacturer's instructions [15].

Syringes of different size were used as homogeneity phantoms: 5 ml syringe (approximately matching the size of the mouse brain, inner diameter 12 mm), 20 ml (rat brain, inner diameter 19 mm) and 50 ml (mouse thorax, inner diameter 27 mm). The syringes were filled with ~50 MBq/ml of ^{99m}Tc. Every syringe was scanned in each acquisition mode with the same net duration (resulting in different total scan duration due to dead time during detector motion). One million counts were collected in each scan in order to achieve good statistical image quality.

The total activity in each SPECT image was obtained by summing all activity within a large region of interest (ROI) including the whole syringe. This value was compared to the true total activity measured in the activimeter. Radioactive decay was taken into account. The PMOD software package was used for ROI analysis (*PMOD Technologies Ltd*., *Zurich*, *Switzerland*).

Reconstructed images were assessed for the presence of artefacts by visual inspection.

Noise Propagation

A 5-ml syringe was filled with 0.5 MBq/ml of ^{99m}Tc and scanned in each acquisition mode. The net frame duration was the same for each mode (resulting in different total scan duration as a function of dead time during detector motion), except for a small prolongation from scan to scan to correct for the radioactive decay. Different frame durations were used to simulate different levels of statistical noise.

A cylindrical ROI with 4 mm radius was placed in the reconstructed image of the syringe. The distance to the edge of the inner volume of the syringe was 2 mm. This corresponds to about three times the FWHM and, therefore, is sufficient to minimize partial volume effects. The ROI also did not include voxels affected by the spatial distortions caused by the stationary acquisition mode (see below) because the variation of the voxel intensities due to these spatial distortions is a systematic error rather than statistical noise. The relative level of statistical noise was characterized by the coefficient of variance CV [%]=100×standard deviation/mean of voxel intensities within the ROI.

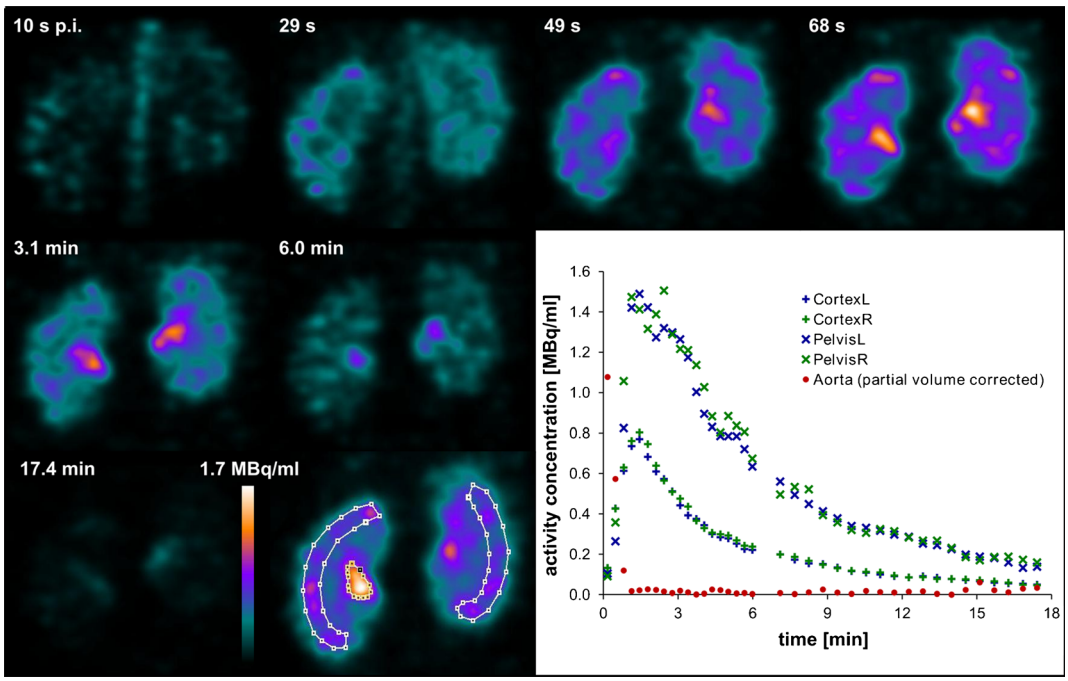

Fig. 4. Dynamic ^{99m}Tc-MAG3 SPECT in a healthy mouse acquired in semi-stationary acquisition mode (Supplementary movie online). Time resolution was improved by intersampling, i.e., reconstruction of the second projection of the first frame with the first projection of the second frame, etc. (N frames each with two projections result in 2N-1 reconstructed images). Time activity curves for cortex and pelvis of left (*L*) and right (*R*) kidney were obtained by three-dimensional ROIs manually placed in the SPECT images (*white contours* shown in a summed image). The time activity curve of the blood was obtained from the aorta and corrected for partial volume effects by the model-free approach described in [19]. Fit of a single exponential to the first four data points of the blood curve (corresponding to the time interval 0–80 s p.i.) showed a half-life of the ^{99m}Tc-MAG3 clearance from blood of about 15 s. The initial slope of the ^{99m}Tc-MAG3 uptake of the kidney cortex was 0.8 MBq/ml/min as obtained by fitting a straight line to the first three data points of the time activity curve (0–60 s p.i.). There was no difference between left and right kidney. The time to the peak of the cortex time activity curve was about 1.5 min for both kidneys, and the peak activity was about 3 % of the injected dose per ml. These values are in good agreement with the results of Tantawy and co-workers who performed dynamic ^{99m}Tc-MAG3 scintigraphy in mice in planar acquisition mode [20].

Jaszczak Phantom

A micro Jaszczak phantom with six fields of rods with 1.0–1.5 mm internal diameter was filled with 90 MBq/ml ^{99m}Tc and scanned in each acquisition mode for a net duration of 60 min. Radioactive decay between the three scans was accounted for by prolonged frames. The RH aperture was used.

In vivo Application

For proof-of-principle, dynamic semi-stationary SPECT was performed in one healthy male C57BL/6 mouse (age, 38 days; 22.2 g) after i.v. injection of ^{99m}Tc-MAG3 into a tail vein (aperture MH, 27.0 MBq in 200 μl) [16]. A low-dose CT scan was used to position the mouse so that both kidneys were within the 14-mm axial FOV of the dynamic SPECT. The dynamic acquisition consisting of 10 frames of 20 s (10 s per detector position) followed by 10 frames of 50 s (25 s per detector position) was initiated at the time of tracer injection.

The animal experiment was approved by the local Committee for Animal Care (*Landesamt für Gesundheit und Soziales Berlin*) and conducted in accordance with the German Animal Protection Act of 18 May 2006 (BGBl. I S. 1206, 1313), last changed 09 December 2010.

Results and Discussion

The results of the measurements of spatial resolution are summarized in Table 1. For the conventional acquisition mode, the estimated FWHM is in good agreement with the specification of the manufacturer [17]: we found 1.16 mm versus a specification of 1.23 mm for RH and 0.69 versus 0.73 mm for MH (^{99m}Tc). Spatial resolution improved with decreasing pinhole diameter. This effect was more pronounced in the rat than in the mouse apertures. The aperture MU for ultra-high resolution in the mouse cannot be recommended for fast dynamic scans because the small increase of spatial resolution compared to the high resolution aperture MH (0.07 mm FWHM for ^{99m}Tc in conventional mode) is associated with considerable reduction of counting efficiency by 75 %. The semi-stationary and stationary acquisition mode caused a slight degradation of the FWHM by 0.04 and 0.07 mm compared to the conventional mode (^{99m}Tc, mean over all apertures). Spatial resolution was slightly worse with ^{123}I than with ^{99m}Tc (on average 0.03 mm), as expected because of the higher photon energy.

The semi-stationary acquisition mode resulted in a very slight underestimation of the activity by about 3 % compared to the conventional mode, consistently in all syringes (Fig. 1). The underestimation was somewhat larger in the stationary mode (about 13 %). The effect of the syringe size on the accuracy of the quantification may be explained by the different apertures (calibration factors) and photon attenuation in the syringe.

Visual evaluation of the syringe images revealed rather strong spatial distortion at the edges of the syringes as well as streak artefacts in stationary mode whereas image quality was not compromised in semi-stationary mode (Fig. 2). The finding of spatial distortions of the reconstructed images in stationary mode was confirmed by the Jaszczak phantom measurements (Fig. 2). This indicates that a minimum of two detector positions is required to avoid noticeable image artefacts by angular undersampling. The artefacts in the stationary mode were much more pronounced in the 50-ml syringe than in the 5-ml syringe. This is explained by the fact that larger objects in general require more angular sampling to avoid aliasing effects. Increasing overlap of independent projections in the multiplexing multi-pinhole acquisition might also contribute to this size dependency [18].

The results of the present study on noise propagation are summarized in Fig. 3. The statistical noise in the reconstructed image was significantly smaller with the semi-stationary acquisition mode than with the conventional mode, particularly at very low count statistics (Fig. 3a). This is most likely a consequence of the fact that the total number of counts is split to a smaller number of projections in the semi-stationary acquisition mode than in the conventional mode so that each single projection has a better statistical quality ("Introduction" section). The stationary mode provided further reduction of statistical noise in the images. The effect of the acquisition mode on image noise is even more pronounced when the dead time due to detector motion is taken into account (Fig. 3b).

Images and time activity curves from the ^{99m}Tc-MAG3 mouse study suggest adequate time resolution for the evaluation of kidney function in the mouse by semi-stationary SPECT (Fig. 4). This was confirmed by a dynamic ^{99m}Tc-MAG3 SPECT study in another healthy C57BL/6 mouse (data not shown).

Conclusions

The semi-stationary acquisition mode significantly improves the capability of the nanoSPECT/CTplus for fast dynamic imaging. Degradation of image quality at high count statistics is negligible. The full stationary acquisition mode causes spatial distortion and streak artefacts, particularly in case of large objects, and, therefore, should be restricted to applications requiring highest temporal resolution.

Conflict of Interest. The authors declare that they have no conflict of interest.

References

1. Vallabhajosula S (2009) Pharmacokinetics and modeling, Molecular imaging: radiopharmaceuticals for PET and SPECT. Springer, Berlin, pp 205–214
2. Neyt S, Huisman MT, Vanhove C et al (2013) *In vivo* visualization and quantification of (disturbed) Oatp-mediated hepatic uptake and Mrp2-mediated biliary excretion of 99mTc-mebrofenin in mice. J Nucl Med 54(4):624–630
3. Franc BL, Acton PD, Mari C, Hasegawa BH (2008) Small-animal SPECT and SPECT/CT: important tools for preclinical investigation. J Nucl Med 49(10):1651–1663
4. Rowland DJ, Cherry SR (2008) Small-animal preclinical nuclear medicine instrumentation and methodology. Semin Nucl Med 38(3):209–222

5. de Kemp RA, Epstein FH, Catana C et al (2010) Small-animal molecular imaging methods. J Nucl Med 51(S1):18S–32S
6. Beekman FJ, Vastenhouw B (2004) Design and simulation of a high-resolution stationary SPECT system for small animals. Phys Med Biol 49(19):4579–4592
7. Furenlid LR, Wilson DW, Chen YC et al (2004) FastSPECT II: a second-generation high-resolution dynamic SPECT imager. IEEE Trans Nucl Sci 51(3):631–635
8. van der Have F, Vastenhouw B, Ramakers RM et al (2009) U-SPECT-II: an ultra-high-resolution device for molecular small-animal imaging. J Nucl Med 50(4):599–605
9. Vaissier PE, Goorden MC, Vastenhouw B et al (2012) Fast spiral SPECT with stationary gamma-cameras and focusing pinholes. J Nucl Med 53(8):1292–1299
10. Schramm NU, Ebel G, Engeland U et al (2003) High-resolution SPECT using multipinhole collimation. IEEE Trans Nucl Sci 50(3):315–320
11. Finucane CM, Murray I, Sosabowski JK et al (2011) Quantitative accuracy of low-count SPECT imaging in phantom and *in vivo* mouse studies. Int J Mol Imaging 2011:197381
12. Deleye S, Van Holen R, Verhaeghe J et al (2013) Performance evaluation of small-animal multipinhole mu SPECT scanners for mouse imaging. Eur J Nucl Med Mol Imaging 40(5):744–758
13. Gordon I, Piepsz A, Sixt R (2011) Guidelines for standard and diuretic renogram in children. Eur J Nucl Med Mol Imaging 38(6):1175–1188
14. Magota K, Kubo N, Kuge Y et al (2011) Performance characterization of the Inveon preclinical small-animal PET/SPECT/CT system for multimodality imaging. Eur J Nucl Med Mol Imaging 38(4):742–752
15. Forrer F, Valkema R, Bernard B et al (2006) *In vivo* radionuclide uptake quantification using a multi-pinhole SPECT system to predict renal function in small animals. Eur J Nucl Med Mol Imaging 33(10):1214–1217
16. Fritzberg AR, Kasina S, Eshima D, Johnson DL (1986) Synthesis and biological evaluation of technetium-99m MAG3 as a hippuran replacement. J Nucl Med 27(1):111–116
17. Bioscan (2011) NanoSPECT/CT technical specification—apertures. Bioscan, Washington
18. Mok GS, Wang Y, Tsui BM (2009) Quantification of the multiplexing effects in multi-pinhole small animal SPECT: a simulation study. IEEE Trans Nucl Sci 56(5):2636–2643
19. Hofheinz F, Langner J, Petr J et al (2012) A method for model-free partial volume correction in oncological PET. EJNMMI Res 2(1):16
20. Tantawy MN, Jiang R, Wang F et al (2012) Assessment of renal function in mice with unilateral ureteral obstruction using 99mTc-MAG3 dynamic scintigraphy. BMC Nephrol 13:168